Resonance Formation in the $\pi^+\pi^-\pi^0$ Final State in Two-Photon Collisions

The L3 Collaboration

Abstract

A study of resonance formation is presented in the $\pi^+\pi^-\pi^0$ final state in two-photon collisions at LEP. The $a_2(1320)$ radiative width is measured to be $\Gamma_{\gamma\gamma} = 0.98 \pm 0.05 \pm 0.09$ keV. The helicity 2 production is dominant. Exclusive $\pi^+\pi^-\pi^0$ production has also been studied in the mass region above the a_2 in the $\rho\pi$ and $f_2\pi$ channels. This region is dominated by a $J^P=2^+$ helicity 2 wave.

1 Introduction

A study of $\pi^+\pi^-\pi^0$ production in two-photon collisions is presented using data taken from 1991 to 1995 by the L3 experiment [1] at a center-of-mass energy $\simeq 91$ GeV. The corresponding integrated luminosity is 140.6 pb^{-1}. The previous measurements of this process [2–9] have focused on the formation of the $a_2(1320)$ meson with well established quantum numbers $\mathrm{J^{PC}}{=}2^{++}$ decaying dominantly into $\rho\pi$. In addition the Crystal Ball [10] and CELLO [7] collaborations have reported the formation of the $\pi_2(1670)$ meson (Crystal Ball in the $\pi^0\pi^0\pi^0$ channel). The π_2 meson is a 2^{-+} tensor state in the $q\bar{q}$ model. A nonrelativistic quark-model calculation [11] predicts a radiative width two to three orders of magnitude smaller than those reported ($\Gamma_{\gamma\gamma} = 1.35 \pm 0.26$ keV [12], average of Crystal Ball and CELLO measurements). Calculations of relativistic quark-models for two-photon decays of mesons [13, 14] also predict a width an order of magnitude lower. A recent partial wave analysis of the $\pi^+\pi^-\pi^0$ system from ARGUS [9] has found no evidence of $\mathrm{J^P}{=}2^-$ $\rho\pi$ and $f_2\pi$ states, with an upper limit of $\Gamma_{\gamma\gamma}(\pi_2) < 0.19$ keV (90% C.L.).

In e^+e^- storage ring experiments the cross section for resonance formation in untagged two-photon collisions can be formulated as the product of the two-photon luminosity function [15] that describes the flux of transverse photons and the resonance cross section given by the Breit-Wigner formula. The $\pi^+\pi^-\pi^0$ final state can be expressed as a set of two body intermediate states with orbital angular momentum L between a di-pion state and the third pion. The a_2 meson decays into $\pi^+\pi^-\pi^0$ through the $\rho^\pm\pi^\mp$ intermediate states with constructive interference [16]; $\rho^0\pi^0$ is forbidden by isospin invariance. For the decay of a candidate high-mass resonance, the intermediate states $\rho^\pm\pi^\mp$ and $f_2\pi^0$ are considered. The angular distribution depends on the spin-parity and helicity of the resonant state X. It is given by

$$\mathcal{T} = \sum_\lambda R_{\lambda\lambda} \left| \left(\frac{T_\lambda(X \to \rho^+\pi^- \to 3\pi)}{m_\rho^2 - s_+ - im_\rho\Gamma_\rho} + \frac{T_\lambda(X \to \rho^-\pi^+ \to 3\pi)}{m_\rho^2 - s_- - im_\rho\Gamma_\rho} \right) \right.$$
$$\left. + \alpha \exp(i\phi) \left(\frac{T_\lambda(X \to f_2\pi^0 \to 3\pi)}{m_{f_2}^2 - s_0 - im_{f_2}\Gamma_{f_2}} \right) \right|^2, \tag{1}$$

where $R_{\lambda\lambda}$ is the probability of the helicity λ state, $s_\pm, s_0$ are the invariant mass squared of the $\pi^\pm\pi^0, \pi^+\pi^-$ systems corresponding to $\rho^\pm$ and f_2. α is defined as the $\sqrt{BR(f_2\pi)/BR(\rho\pi)}$, and ϕ is the relative phase of the $f_2\pi$ and $\rho\pi$ decay amplitudes. For the a_2, $\alpha{=}0$. The transition amplitude T_λ is given by

$$T_\lambda = 32\pi^2 \left(m_X \Gamma_X \, m_{2\pi}\Gamma_{2\pi} \frac{W_{\gamma\gamma}\sqrt{s_{2\pi}}}{p_{2\pi}p_\pi} \right)^{1/2} \times \sum_m C_{L,\lambda-m,l,m}^{J\lambda} Y_L^{\lambda-m}(\theta_{2\pi}, \phi_{2\pi}) Y_l^m(\theta_\pi, \phi_\pi), \tag{2}$$

where Γ_X is the X decay width at the resonance invariant mass $W_{\gamma\gamma}$, m_X is the resonance pole mass. The di-pion system has spin l with third component m, the invariant mass is $m_{2\pi}$ with the mass dependent width $\Gamma_{2\pi}$. The momentum, polar and azimuthal angles $(p_{2\pi}, \theta_{2\pi}, \phi_{2\pi})$ are measured in the $\gamma\gamma$ rest frame. The π from the di-pion decay has the corresponding variables $(p_\pi, \theta_\pi, \phi_\pi)$ measured in the di-pion rest frame. The angles in both frames are determined with respect to the $\gamma\gamma$ direction which is approximately the beam direction. The mass-dependent widths of the a_2, f_2 and ρ are given by Ref. [17]. Spin-parity $\mathrm{J^P}{=}1^\pm$ and $\mathrm{J^P}(\lambda){=}2^-(2)$ are excluded by the Landau-Yang theorem [18], and a $\mathrm{J^P}{=}0^+$ state cannot decay into 3π by parity conservation.

2   Event selection and background estimations

The process $e^+e^- \rightarrow e^+e^-\pi^+\pi^-\pi^0$ has been selected in an untagged configuration. The p_T threshold for charged track selection is 60 MeV. The energy of a photon candidate is required to be greater than 80 MeV with an angular separation from charged tracks of $(\Delta\theta^2+\Delta\phi^2)^{1/2} > 5.5°$. Photon candidates are selected in the angular regions $14° < \theta < 35°$, $45° < \theta < 135°$, or $145° < \theta < 166°$. The π^0 signal region is defined as $105 < m(\gamma\gamma) < 165$ MeV, where $m(\gamma\gamma)$ is the invariant mass of the two photons.

The transverse momentum of the $\pi^+\pi^-\pi^0$ system relative to the beam direction is denoted by $\sum\vec{p}_T$. The mass spectra with $|\sum\vec{p}_T|^2$ below and above 0.0015 GeV^2 are shown in Fig. 1. The distribution is dominated by the a_2. One sees that the mass resolution deteriorates and the background increases at higher values of $|\sum\vec{p}_T|^2$. Fig. 2a to 2d show the $|\sum\vec{p}_T|^2$ distributions for different $\pi^+\pi^-\pi^0$ mass intervals. In the mass intervals 1.0-1.55 GeV and 1.55-2.1 GeV there is a clear excess of events at low $|\sum\vec{p}_T|^2$ corresponding to exclusive $\pi^+\pi^-\pi^0$ production. The almost flat background extending to large $|\sum\vec{p}_T|^2$ values is interpreted as inclusive production. The shaded histogram in Fig. 2c shows the prediction of a Monte Carlo phase space generation of the channel $\pi^+\pi^-\pi^0(\pi^0)$ where the last π^0 is unobserved. This describes correctly the shape of the distribution for large $|\sum\vec{p}_T|^2$.

To estimate the statistical significance of the exclusive signals several fits were performed to the $|\sum\vec{p}_T|^2$ distributions below 0.02 GeV^2. The results and confidence levels of "background only" fits to a second order polynomial are given in the first two rows of Table 1. To estimate the levels of the inclusive backgrounds under the exclusive production signals in Figs. 2b,c the distributions were fitted to the sum of a Monte Carlo distribution including the effect of a ρ dominated Vector-Meson-Dominance (VMD) form factor to describe the exclusive signal, and a second order polynomial to describe the inclusive background. As listed in the third row of Table 1, acceptable fits are then obtained. The background levels for $|\sum\vec{p}_T|^2 < 0.0015$ GeV^2 of the fits are listed in the last three rows of Table 1.

mass region [GeV]	$0.60 - 1.00$	$1.00 - 1.55$	$1.55 - 2.10$	$2.10 - 2.50$
χ^2 (Background)	105	585	221	92
C.L.[%]	95	$< 10^{-6}$	1.1×10^{-4}	99
χ^2 (MC+Background)	–	157	155	–
C.L.[%]	–	5.4	6.7	–
Total events	42	618	184	38
Background events	–	120	46	–
Background fraction [%]	–	19±0.5	25±3	–

Table 1: The $|\sum\vec{p}_T|^2$ distributions below 0.02 GeV^2 in the four mass ranges are fitted to background only (first two rows) and Monte Carlo plus background (third and fourth rows). The χ^2 for 130 D.F. are listed. The fraction of background events in $|\sum\vec{p}_T|^2 < 0.0015$ GeV^2 are also listed with the number of events observed.

In the spin-parity-helicity analyses presented below, events with $|\sum\vec{p}_T|^2 < 0.0015$ GeV^2 are divided into two samples. The a_2 *low-mass* sample is selected with $\pi^+\pi^-\pi^0$ invariant mass of $1.0 < m(\pi^+\pi^-\pi^0) < 1.55$ GeV. The $\pi^\pm\pi^0$ invariant mass is required to be compatible with the ρ mass $(m(\pi^\pm\pi^0) < m_\rho + 250$ MeV) since the a_2 decays predominantly through the $\rho\pi$ intermediate state (see Fig. 3). The *high-mass* sample of $1.55 < m(\pi^+\pi^-\pi^0) < 2.1$ GeV is

studied under the hypothesis of a resonance (or resonances) decaying through $\rho\pi$ and $f_2\pi$.

The detector acceptance and event selection efficiency for different spin-parity and helicity states have been evaluated by Monte Carlo simulations using the PC [19] and TWOGEN [20] generators with a ρ dominated VMD form factor applied for the colliding photons. The mass and total width for the a_2 are taken from the Particle Data Group (PDG) [12]. In the high-mass range a Breit-Wigner resonance of mass 1740 MeV and total width 150 MeV have been assumed. Monte Carlo events were passed through a full detector simulation. The detector acceptances for $|\sum \vec{p}_T|^2 < 0.0015$ GeV^2 calculated for different intermediate states and spin-parity assignments are listed in Table 2. For the high-mass region the amplitude and phase parameters α and ϕ determined by the fits described in Section 3 below are used.

	$a_2(1320) \to \rho\pi$			$BW(1740) \to \rho\pi + f_2\pi$			
J$^{\mathrm{P}}(\lambda)$	$2^+(0)$	$2^+(2)$	LIPS	$2^-(0)$	$2^+(0)$	$2^+(2)$	LIPS
$\mathcal{A}$ [%]	0.41	0.50	0.42	0.72	0.63	0.91	0.58

Table 2: The detector acceptance $\mathcal{A}$ for events with $|\sum \vec{p}_T|^2 < 0.0015$ GeV^2 of different spin-parity-helicity states and Lorentz invariant phase space (LIPS).

3 Spin-parity and helicity analysis

We have analyzed the *low-mass* sample to obtain the helicity state of the a_2. When produced in quasi-real two-photon collisions, the a_2 meson can have helicity states 0 or 2. The relative importance is determined by the least square minimization to the polar angle ($\cos\theta$) distributions of the final state pions in the resonance rest frame where $\theta = \pi - \theta_{2\pi}$. The $\cos\theta$ distributions are sensitive to the helicity state. The Monte Carlo expectations for the $\cos\theta$ distributions of π^0 and $\pi^\pm$ (two entries per event) are given by

$$E_i = P_b \cdot \mathcal{B}_i^\theta + P_{\gamma\gamma} \cdot \{P_2 \cdot M_i(2) + (1 - P_2) \cdot M_i(0)\} \tag{3}$$

where $M_i(\lambda)$ is the bin content of simulated events of helicity λ normalized to the expected number of events for a radiative width $\Gamma_{\gamma\gamma} = 1$ keV. The background distribution $\mathcal{B}_i^\theta$ is taken from the $\pi^+\pi^-\pi^0$ phase space Monte Carlo. The free parameters in the fit are the fraction P_2 of helicity 2 contribution, and the two scaling factors $P_{\gamma\gamma}$ for the radiative width of the resonance and P_b for the background contributions. The P_2 parameter corresponds to $R_{\lambda\lambda}$ in Eq. 1 ($P_2/(1 - P_2) = R_{22}/R_{00}$). The forward regions ($|\cos\theta| > 0.94$) with low acceptance are excluded from the fit. The result of the fit is shown in Fig. 4. We have obtained $P_{\gamma\gamma} = 0.96 \pm 0.04$ and $P_2 = 0.92 \pm 0.05$ with $\chi^2/D.F. = 90/53$ (C.L.=0.11%). The P_b obtained corresponds to $26 \pm 2\%$ of background contamination, which may be compared with the estimated level of inclusive background of $19.0 \pm 0.5\%$ obtained from the fit to the $|\sum \vec{p}_T|^2$ distribution. The excess of 7% of events is used to estimate the rate of s-wave $\pi^+\pi^-\pi^0$ production (possibly $\pi(1300)$ formation). It corresponds to 41 observed events which implies a radiative width of $\Gamma_{\gamma\gamma}BR(\pi^+\pi^-\pi^0) < 0.085$ keV at 90% C.L. for any s-wave contribution.

The fitted parameters are sensitive to the background level. We performed the fit again with the background fraction fixed to 20%. The parameters of the fit are in this case $P_{\gamma\gamma} = 1.05 \pm 0.03$ and $P_2 = 0.87 \pm 0.05$ with $\chi^2/D.F. = 90/54$ (C.L.=0.15%). The total systematic uncertainty in P_2 is estimated to be 6% and has dominant contributions from background uncertainty and detector acceptance, each estimated to be 4%.

In the *high-mass* sample we observe 184 events. The intermediate decay modes $\rho\pi$ and $f_2\pi$ are considered for the exclusive signal. The coherent interference of the two intermediate states $\rho\pi$ and $f_2\pi$ is expressed in Eq. 1. We first analyze the spin-parity state using the Dalitz Λ parameter [21] defined in the $\pi^+\pi^-\pi^0$ rest frame by

$$\Lambda = \left| \frac{\mathbf{p}_{\pi^+} \times \mathbf{p}_{\pi^-}}{Q_K^2} \right|^2 \tag{4}$$

where the $\pi^\pm$ momenta ($\mathbf{p}_{\pi^\pm}$) are normalized to Q_K, the maximum possible kinetic energy for a pion in the event. The Λ distribution is shown as the data points in Fig. 5.

The Dalitz Λ parameter is sensitive to the distribution of the relative angles between the final state pions, and depends on the spin-parity of the state as well as the amplitude and phase parameters α and ϕ. We compare data with Monte Carlo event samples generated with different values of the α and ϕ parameters for each spin-parity-helicity state. A background level of 25% of inclusive events, as determined by the fit to the $|\sum \vec{p}_T|^2$ distribution (Fig. 2), was used. The background is simulated by Monte Carlo $\pi^+\pi^-\pi^0(\pi^0)$ phase space events. Increasing either of these parameters in the Monte Carlo shifts the Λ distribution to lower values. The parameters α and ϕ are determined for each spin-parity and helicity state by minimizing the χ^2 value. The results of the fits are listed in Table 3. For both $2^+(0)$ and $2^+(2)$ the fitted value of α is consistent with one. In all cases the phase angle is large ($> 90°$) and for $2^+(2)$ is consistent with $\phi = 180°$ ($f_2\pi$ and $\rho\pi$ amplitudes relatively real). No acceptable fit was found for $2^-(0)$. The spin-parity $\mathrm{J^P} = 2^+$ is strongly favored. This fit is not, however, sensitive to the helicity state.

Comparisons are also made for different α and ϕ values with the effective mass spectra of the intermediate $\pi^\pm\pi^0$ and $\pi^+\pi^-$ states. The mass peak positions also move as the phase angle increases; the $\pi^\pm\pi^0$ mass toward lower values and the $\pi^+\pi^-$ mass in the opposite direction. The α and ϕ parameters determined are consistent with those obtained from the Λ distributions. The di-pion mass spectra of the intermediate states are shown in Fig. 6 in comparison with the Monte Carlo predictions for different $\mathrm{J^P}(\lambda)$ assignments.

$\mathrm{J^P}(\lambda)$	$2^-(0)$	$2^+(0)$	$2^+(2)$
phase angle ϕ [deg.]	100	130 ± 18	170 ± 17
amplitude α	1.0	0.99 ± 0.10	0.97 ± 0.17
$\chi^2/15$ D.F.	3.94	0.83	0.61
C.L. [%]	3.6×10^{-5}	64	87

Table 3: Results of fits to the Λ distribution.

The helicity state can be 0 or 2 as for the a_2 with different angular distributions in the $\pi^+\pi^-\pi^0$ rest frame. Fig. 7 shows the $\cos\theta$ distributions for π^0 and $\pi^\pm$ (two entries per event). The data is fitted to Monte Carlo expectations of pure $2^-(0)$, $2^+(0)$, $2^+(2)$ states and inclusive $\pi^+\pi^-\pi^0(\pi^0)$ background :

$$E_i = P_b \cdot \mathcal{B}_i^\theta + P_{\gamma\gamma} \cdot \left\{ (1 - F_{2^-}) \left[P_2 M_i^+(2) + (1 - P_2) M_i^+(0) \right] + F_{2^-} M_i^-(0) \right\}. \tag{5}$$

The inclusive background is parameterized by $\mathcal{B}_i^\theta$ and scaled by P_b. $P_{\gamma\gamma}$ and P_2 are defined as in Eq. 3. The parameter F_{2^-} is the relative contribution of the $2^-(0)$ state. The results of the fits are listed in table 4. Assuming a pure $2^-(0)$ state gives a low C.L. of 1.7×10^{-8}

(column I). The fitted values of the background level and P_2 are $23 \pm 4\%$ and $77 \pm 12\%$ respectively (column II). The fitted background is consistent with that derived from the $|\sum \vec{p}_T|^2$ distributions ($25 \pm 3\%$, Table. 1). A fit is also performed with background level fixed at 23% and the $2^-(0)$ contribution left free (column III). The upper limit for a possible $2^-(0)$ contribution is $\Gamma_{\gamma\gamma}\mathrm{BR}(\pi^+\pi^-\pi^0) \leq 0.072$ keV (90% C.L.).

The systematic errors in P_2 given by uncertainties in detector acceptance, background levels, and the uncertainty in the $\rho\pi/f_2\pi$ branching ratio are estimated to contribute 4% each, for a total of 7%.

	I	II	III
Background [%]	0^*	23 ± 4	23^*
P_2 [%]	$-$	77 ± 12	74 ± 13
$2^-(0)$ [%]	100^*	0^*	12 ± 11
$P_{\gamma\gamma}$ [keV]	0.43 ± 0.02	0.38 ± 0.03	0.39 ± 0.02
C.L. [%]	1.7×10^{-6}	57	61

Table 4: Parameters of fits to $\cos\theta$ distributions of π^0 and $\pi^\pm$. (*) parameter fixed in the fit.

4   Resonance parameters

The $m(\pi^+\pi^-\pi^0)$ mass spectrum in the region 1.0-2.1 GeV with $|\sum \vec{p}_T|^2 < 0.0015$ GeV^2 is fitted by minimizing a χ^2 function with expected value in bin i of :

$$E_i = \Gamma_{\gamma\gamma}^{a_2} \cdot M_i^{a_2} + BW_i + P_b \mathcal{B}_i^m. \qquad (6)$$

The a_2 contribution, represented by $M_i^{a_2}$, is given by the Monte Carlo, assuming the PDG average values of the mass and width [12], and helicity 2 fraction $P_2 = 0.92$, as determined in Section 3 above. The a_2 contribution is scaled by the factor $\Gamma_{\gamma\gamma}^{a_2}$, which is a free parameter in the fit. The high-mass exclusive signal is described by the Breit-Wigner function:

$$BW = P_{BW} \cdot \frac{\Gamma_{tot}}{(m^2 - W_{\gamma\gamma}^2)^2 + m^2\Gamma_{tot}^2}, \qquad (7)$$

with fit parameters P_{BW}, Γ_{tot} and m. The detector acceptance is folded in P_{BW}. The inclusive background $\mathcal{B}_i^m$ is estimated from the fits to the $|\sum \vec{p}_T|^2$ distributions shown in Fig. 2. The shape is parameterized by a third order polynomial with the normalization P_b left free in the fit. The result of the fit is shown in Fig. 8, with $\chi^2 = 57$ for 42 D.F. (C.L.=6.1%).

The radiative widths for a_2 and the events in the high-mass region described by Eq. 7 are obtained from the fitted parameters $\Gamma_{\gamma\gamma}^{a_2}$ and P_{BW}. The normalization factor P_b of the background obtained from the fit is 0.94 ± 0.10, which is consistent with the level estimated from the $|\sum \vec{p}_T|^2$ distributions. The fitted widths are $\Gamma_{\gamma\gamma} = 0.98 \pm 0.05$ for the a_2 and $\Gamma_{\gamma\gamma}BR(\pi^+\pi^-\pi^0) = 0.29 \pm 0.04$ for the high-mass region assuming a single resonance. For the a_2, the radiative width is consistent with that obtained from the angular distribution (Section 3). The systematic errors in the radiative widths are due to uncertainties in acceptance, background, and branching ratios. For the a_2 these contributions are 3%, 4% and 7%, respectively; while for the high-mass region they are 4% for acceptance and 4% for background. These values are summarized in Table 5.

The fitted resonance parameters are corrected for the calibration estimated by the Monte Carlo simulations. The mass-dependent width introduces a mass shift of -11 ± 1 MeV at $m=1320$ MeV and -20 ± 2 MeV at $m=1750$ MeV. The photon energy and track momentum measurements both have a slight offset to lower values of the order of 1%, which are determined by the effective mass distributions of inclusive $\pi^0 \to \gamma\gamma$ and $K_s \to \pi^+\pi^-$, respectively. The combined offsets for $\pi^+\pi^-\pi^0$ are estimated by the Monte Carlo to be -2 ± 3 and -12 ± 3 MeV at 1320 and 1750 MeV, respectively. The systematic uncertainty is the combined error of the two shifts. For the high-mass region the corrected mass is $m = 1752 \pm 21 \pm 4$ MeV. We also made a separate Breit-Wigner fit for the mass and width of the a_2. The mass is found to be $1323 \pm 4 \pm 3$ MeV. The mass resolution of the detector increases the Γ values obtained in the Breit-Wigner fits. This effect is calculated using Monte Carlo. The corrections to Γ are -38 ± 11 MeV and -60 ± 34 MeV for the a_2 and at 1750 MeV, respectively; the corrected widths are $\Gamma = 105 \pm 10 \pm 11$ MeV and $\Gamma = 150 \pm 110 \pm 34$ MeV, respectively.

The resonance parameters and the relative importance of the helicity 2 state (P_2) (Section 3) in the two mass regions are summarized in Table 5. The large error on the fitted width for the high-mass region and the apparent excesses of events relative to the fitted curve around 1.5 GeV and 1.85 GeV indicates that the single Breit-Wigner fit should be considered only as a rough description of the data in the high-mass region.

	$a_2(1320)$	high-mass region
$\Gamma_{\gamma\gamma}$ [keV]	$0.98 \pm 0.05 \pm 0.09$	–
$\Gamma_{\gamma\gamma}BR(\rho\pi + f_2\pi)$ [keV]	–	$0.29 \pm 0.04 \pm 0.02$
m [MeV]	$1323 \pm 4 \pm 3$	$1752 \pm 21 \pm 4$
Γ [MeV]	$105 \pm 10 \pm 11$	$150 \pm 110 \pm 34$
P_2 [%]	$92 \pm 5 \pm 5$	$77 \pm 12 \pm 5$

Table 5: The resonance parameters and the corresponding statistical and systematic errors.

5   Discussion and conclusions

The $\pi^+\pi^-\pi^0$ final state in two-photon collisions is found to be dominated by formation of the a_2 meson. The resonance mass and total width and radiative width (Table 5) obtained are in good agreement with the current world average values [12]. The $\lambda=2$ helicity state is dominant. A upper limit for s-wave contribution is estimated to be $\Gamma_{\gamma\gamma}BR(\pi^+\pi^-\pi^0) < 0.085$ keV (90% C.L.).

The $\pi^+\pi^-\pi^0$ events in the high-mass region (1.55-2.1) GeV have been analyzed for spin-parity and resonance parameters for spin up to J=2 and in intermediate states $\rho\pi$ and $f_2\pi$. From the analysis of the Λ parameter distribution and the pion $\cos\theta$ distributions, the spin-parity of the selected exclusive events are found to be dominated by $J^P(\lambda) =2^+(2)$. Equal branching ratios for decays into the $f_2\pi$ and $\rho\pi$ final states are observed and the phase angle ϕ between the $\rho\pi$ and $f_2\pi$ amplitudes is consistent with $180°$. The results may be compared with theoretical predictions, in particular the calculations of the relativistic quark model of Ref. [14]. If these events are identified with the first radial excitation of the a_2, the fitted mass $m = 1752 \pm 21 \pm 4$ MeV is consistent only with the One Gluon Exchange Semi-Relativistic Quark Mass (OGE-SRM) model which predicts a mass of 1740 MeV. All the models of Ref. [14] give values of $\Gamma_{\gamma\gamma}(a_2')$ in the range 0.33-0.38 keV, compatible with our measurement $\Gamma_{\gamma\gamma}BR(\pi^+\pi^-\pi^0) =$

$0.29 \pm 0.04 \pm 0.02$ MeV, on the assumption that 3π decay mode is the dominant one. The presence of several overlapping states in the high-mass region cannot be excluded. The OGE-SRM model predicts a second radial recurrence of the a_2 at 1820 MeV where a small data excess is seen. Higher statistics are needed to better understand this mass region.

The formation of a $\mathrm{J^P} = 2^-$ state, π_2, claimed by previous collaborations [7, 10] was based solely on the 3π mass distribution and observation of $f_2\pi$ decay mode. No evidence is seen for this state. The upper limit $\Gamma_{\gamma\gamma}(\pi_2)BR(\pi^+\pi^-\pi^0) < 0.072$ keV (90% C.L.) is found. This result is in agreement with the ARGUS observation [9]. We conclude that the spin-parity of $\pi^+\pi^-\pi^0$ final states in this mass region is actually dominated by $\mathrm{J^P} = 2^+$ with helicity $\lambda = 2$. The measured two-photon width is consistent with the theoretical predictions [11, 13, 14] for a radially excited a_2 state.

Acknowledgement

References

[1] L3 Collab., B. Adeva et al., Nucl. Inst. Meth. A 289 (1990) 35.

[2] JADE Collab., J.E. Olsson, in Proc. V Int. Conf. on Two-Photon Physics, Aachen 1983 ed. Ch. Berger (Springer, Berlin 1983).

[3] CELLO Collab., H.J. Behrend et al., Phys. Lett. 114B (1982) 378; Phys. Lett. 125B (1983) 518.

[4] PLUTO Collab., Ch. Berger et al., Phys. Lett. 149B (1984) 427.

[5] TASSO Collab., M. Althoff et al., Z. Phys. C 31 (1986) 537.

[6] MARK2 Collab., F. Butler et al., Phys. Rev. D 42 (1990) 1368.

[7] CELLO Collab., H.J. Behrend et al., Z. Phys. C 46 (1990) 583.

[8] MD1 Collab., S.E. Baru et al., Z. Phys. C 48 (1990) 581.

[9] ARGUS Collab., H. Albrecht et al., DESY 96-015 Jan. 1996; DESY 96-112 Jun. 1996.

[10] Crystal Ball Collab., D. Antreasyan et al., Z. Phys. C 48 (1990) 561.

[11] J.D. Anderson et al., Phys. Rev. D 43 (1991) 2094.

[12] Review of Particle Physics, Phys. Rev. D 54 (1996) 1.

[13] E.S. Ackleh et al., Phys. Rev. D45 (1992) 232.

[14] C.R. Münz, Nucl. Phys. A 609 (1996) 364.

[15] V.M. Budnev et al., Phys. Rep. 15 (1975) 181.

[16] W.R.Frazer et al., Phys. Rev. 136 (1964) B1207.

[17] J.D. Jackson, Nuovo Cimento 34 (1964) 1644.

[18] L.D. Landau, Sov. Phys. Doklady 60 (1948) 207; C.N. Yang, Phys. Rev. 77 (1950) 242.

[19] F.L. Linde, Ph.D. thesis (Rijksuniversiteit Leiden, 1988).

[20] A. Buijs et al., Comp. Phys. Comm. 79 (1994) 523.

[21] G. Goldhaber et al., Phys. Rev. Lett. 15 (1965) 118.

The L3 Collaboration:

M.Acciarri,[28] O.Adriani,[17] M.Aguilar-Benitez,[27] S.Ahlen,[11] J.Alcaraz,[27] G.Alemanni,[23] J.Allaby,[18] A.Aloisio,[30] G.Alverson,[12] M.G.Alviggi,[30] G.Ambrosi,[20] H.Anderhub,[50] V.P.Andreev,[39] T.Angelescu,[13] F.Anselmo,[9] A.Arefiev,[29] T.Azemoon,[3] T.Aziz,[10] P.Bagnaia,[38] L.Baksay,[45] R.C.Ball,[3] S.Banerjee,[10] Sw.Banerjee,[10] K.Banicz,[47] A.Barczyk,[50,48] R.Barillère,[18] L.Barone,[38] P.Bartalini,[35] A.Baschirotto,[28] M.Basile,[9] R.Battiston,[35] A.Bay,[23] F.Becattini,[17] U.Becker,[16] F.Behner,[50] J.Berdugo,[27] P.Berges,[16] B.Bertucci,[35] B.L.Betev,[50] S.Bhattacharya,[10] M.Biasini,[18] A.Biland,[50] G.M.Bilei,[35] J.J.Blaising,[4] S.C.Blyth,[36] G.J.Bobbink,[2] R.Bock,[1] A.Böhm,[1] L.Boldizsar,[14] B.Borgia,[38] A.Boucham,[4] D.Bourilkov,[50] M.Bourquin,[20] D.Boutigny,[4] S.Braccini,[20] J.G.Branson,[41] V.Brigljevic,[50] I.C.Brock,[36] A.Buffini,[17] A.Buijs,[46] J.D.Burger,[16] W.J.Burger,[20] J.Busenitz,[45] X.D.Cai,[16] M.Campanelli,[50] M.Capell,[16] G.Cara Romeo,[9] G.Carlino,[30] A.M.Cartacci,[17] J.Casaus,[27] G.Castellini,[17] F.Cavallari,[38] N.Cavallo,[30] C.Cecchi,[20] M.Cerrada,[27] F.Cesaroni,[24] M.Chamizo,[27] Y.H.Chang,[52] U.K.Chaturvedi,[19] S.V.Chekanov,[32] M.Chemarin,[26] A.Chen,[52] G.Chen,[7] G.M.Chen,[7] H.F.Chen,[21] H.S.Chen,[7] M.Chen,[16] G.Chiefari,[30] C.Y.Chien,[5] L.Cifarelli,[40] F.Cindolo,[9] C.Civinini,[17] I.Clare,[16] R.Clare,[16] H.O.Cohn,[33] G.Coignet,[4] A.P.Colijn,[2] N.Colino,[27] V.Commichau,[1] S.Costantini,[8] F.Cotorobai,[13] B.de la Cruz,[27] A.Csilling,[14] T.S.Dai,[16] R.D'Alessandro,[17] R.de Asmundis,[30] A.Degré,[4] K.Deiters,[48] P.Denes,[37] F.DeNotaristefani,[38] D.DiBitonto,[45] M.Diemoz,[38] D.van Dierendonck,[2] F.Di Lodovico,[50] C.Dionisi,[38] M.Dittmar,[50] A.Dominguez,[41] A.Doria,[30] I.Dorne,[4] M.T.Dova,[19,♯] E.Drago,[30] D.Duchesneau,[4] P.Duinker,[2] I.Duran,[42] S.Dutta,[10] S.Easo,[35] Yu.Efremenko,[33] H.El Mamouni,[26] A.Engler,[36] F.J.Eppling,[16] F.C.Erné,[2] J.P.Ernenwein,[26] P.Extermann,[20] M.Fabre,[48] R.Faccini,[38] S.Falciano,[38] A.Favara,[17] J.Fay,[26] O.Fedin,[39] M.Felcini,[50] B.Fenyi,[45] T.Ferguson,[36] F.Ferroni,[38] H.Fesefeldt,[1] E.Fiandrini,[35] J.H.Field,[20] F.Filthaut,[36] P.H.Fisher,[16] I.Fisk,[41] G.Forconi,[16] L.Fredj,[20] K.Freudenreich,[50] C.Furetta,[28] Yu.Galaktionov,[29,16] S.N.Ganguli,[10] P.Garcia-Abia,[49] S.S.Gau,[12] S.Gentile,[38] J.Gerald,[5] N.Gheordanescu,[13] S.Giagu,[38] S.Goldfarb,[23] J.Goldstein,[11] Z.F.Gong,[21] A.Gougas,[5] G.Gratta,[34] M.W.Gruenewald,[8] V.K.Gupta,[37] A.Gurtu,[10] L.J.Gutay,[47] B.Hartmann,[1] A.Hasan,[31] D.Hatzifotiadou,[9] T.Hebbeker,[8] A.Hervé,[18] W.C.van Hoek,[32] H.Hofer,[50] S.J.Hong,[44] H.Hoorani,[36] S.R.Hou,[52] G.Hu,[5] V.Innocente,[18] H.Janssen,[4] K.Jenkes,[1] B.N.Jin,[7] L.W.Jones,[3] P.de Jong,[18] I.Josa-Mutuberria,[27] A.Kasser,[23] R.A.Khan,[19] D.Kamrad,[49] Yu.Kamyshkov,[33] J.S.Kapustinsky,[25] Y.Karyotakis,[4] M.Kaur,[19,◇] M.N.Kienzle-Focacci,[20] D.Kim,[38] D.H.Kim,[44] J.K.Kim,[44] S.C.Kim,[44] Y.G.Kim,[44] W.W.Kinnison,[25] A.Kirkby,[34] D.Kirkby,[34] J.Kirkby,[18] D.Kiss,[14] W.Kittel,[32] A.Klimentov,[16,29] A.C.König,[32] A.Kopp,[49] I.Korolko,[29] V.Koutsenko,[16,29] R.W.Kraemer,[36] W.Krenz,[1] A.Kunin,[16,29] P.Ladron de Guevara,[27] G.Landi,[17] C.Lapoint,[16] K.Lassila-Perini,[50] P.Laurikainen,[22] M.Lebeau,[18] A.Lebedev,[16] P.Lebrun,[26] P.Lecomte,[50] P.Lecoq,[18] P.Le Coultre,[50] C.Leggett,[3] J.M.Le Goff,[18] R.Leiste,[49] E.Leonardi,[38] P.Levtchenko,[39] C.Li,[21] C.H.Lin,[52] W.T.Lin,[52] F.L.Linde,[2,18] L.Lista,[30] Z.A.Liu,[7] W.Lohmann,[49] E.Longo,[38] W.Lu,[34] Y.S.Lu,[7] K.Lübelsmeyer,[1] C.Luci,[38] D.Luckey,[16] L.Luminari,[38] W.Lustermann,[48] W.G.Ma,[21] M.Maity,[10] G.Majumder,[10] L.Malgeri,[38] A.Malinin,[29] C.Maña,[27] D.Mangeol,[32] S.Mangla,[10] P.Marchesini,[50] A.Marin,[11] J.P.Martin,[26] F.Marzano,[38] G.G.G.Massaro,[2] D.McNally,[18] S.Mele,[30] L.Merola,[30] M.Meschini,[17] W.J.Metzger,[32] M.von der Mey,[1] Y.Mi,[23] A.Mihul,[13] A.J.W.van Mil,[32] G.Mirabelli,[38] J.Mnich,[18] P.Molnar,[8] B.Monteleoni,[17] R.Moore,[3] S.Morganti,[38] T.Moulik,[10] R.Mount,[34] S.Müller,[1] F.Muheim,[20] A.J.M.Muijs,[2] S.Nahn,[16] M.Napolitano,[30] F.Nessi-Tedaldi,[50] H.Newman,[34] T.Niessen,[1] A.Nippe,[1] A.Nisati,[38] H.Nowak,[49] Y.D.Oh,[44] H.Opitz,[1] G.Organtini,[38] R.Ostonen,[22] C.Palomares,[27] D.Pandoulas,[1] S.Paoletti,[38] P.Paolucci,[30] H.K.Park,[36] I.H.Park,[44] G.Pascale,[38] G.Passaleva,[17] S.Patricelli,[30] T.Paul,[12] M.Pauluzzi,[35] C.Paus,[1] F.Pauss,[50] D.Peach,[18] Y.J.Pei,[1] S.Pensotti,[28] D.Perret-Gallix,[4] B.Petersen,[32] S.Petrak,[8] A.Pevsner,[5] D.Piccolo,[30] M.Pieri,[17] J.C.Pinto,[36] P.A.Piroué,[37] E.Pistolesi,[28] V.Plyaskin,[29] M.Pohl,[50] V.Pojidaev,[29,17] H.Postema,[16] N.Produit,[20] D.Prokofiev,[39] G.Rahal-Callot,[50] N.Raja,[10] P.G.Rancoita,[28] M.Rattaggi,[28] G.Raven,[41] P.Razis,[31] K.Read,[33] D.Ren,[50] M.Rescigno,[38] S.Reucroft,[12] T.van Rhee,[46] S.Riemann,[49] K.Riles,[3] O.Rind,[3] A.Robohm,[50] J.Rodin,[16] B.P.Roe,[3] L.Romero,[27] S.Rosier-Lees,[4] Ph.Rosselet,[23] W.van Rossum,[46] S.Roth,[1] J.A.Rubio,[18] D.Ruschmeier,[8] H.Rykaczewski,[50] J.Salicio,[18] E.Sanchez,[27] M.P.Sanders,[32] M.E.Sarakinos,[22] S.Sarkar,[10] M.Sassowsky,[1] G.Sauvage,[4] C.Schäfer,[1] V.Schegelsky,[39] S.Schmidt-Kaerst,[1] D.Schmitz,[1] P.Schmitz,[1] M.Schneegans,[4] N.Scholz,[50] H.Schopper,[51] D.J.Schotanus,[32] J.Schwenke,[1] G.Schwering,[1] C.Sciacca,[30] D.Sciarrino,[20] L.Servoli,[35] S.Shevchenko,[34] N.Shivarov,[43] V.Shoutko,[29] J.Shukla,[25] E.Shumilov,[29] A.Shvorob,[34] T.Siedenburg,[1] D.Son,[44] A.Sopczak,[49] V.Soulimov,[30] B.Smith,[16] P.Spillantini,[17] M.Steuer,[16] D.P.Stickland,[37] H.Stone,[37] B.Stoyanov,[43] A.Straessner,[1] K.Strauch,[15] K.Sudhakar,[10] G.Sultanov,[19] L.Z.Sun,[21] G.F.Susinno,[20] H.Suter,[50] J.D.Swain,[19] X.W.Tang,[7] L.Tauscher,[6] L.Taylor,[12] Samuel C.C.Ting,[16] S.M.Ting,[16] M.Tonutti,[1] S.C.Tonwar,[10] J.Tóth,[14] C.Tully,[37] H.Tuchscherer,[45] K.L.Tung,[7] Y.Uchida,[16] J.Ulbricht,[50] U.Uwer,[18] E.Valente,[38] R.T.Van de Walle,[32] G.Vesztergombi,[14] I.Vetlitsky,[29] G.Viertel,[50] M.Vivargent,[4] R.Völkert,[49] H.Vogel,[36] H.Vogt,[49] I.Vorobiev,[29] A.A.Vorobyov,[39] A.Vorvolakos,[31] M.Wadhwa,[6] W.Wallraff,[1] J.C.Wang,[16] X.L.Wang,[21] Z.M.Wang,[21] A.Weber,[1] F.Wittgenstein,[18] S.X.Wu,[19] S.Wynhoff,[1] J.Xu,[11] Z.Z.Xu,[21] B.Z.Yang,[21] C.G.Yang,[7] X.Y.Yao,[7] J.B.Ye,[21] S.C.Yeh,[52] J.M.You,[36] An.Zalite,[39] Yu.Zalite,[39] P.Zemp,[50] Y.Zeng,[1] Z.Zhang,[7] Z.P.Zhang,[21] B.Zhou,[11] Y.Zhou,[3] G.Y.Zhu,[7] R.Y.Zhu,[34] A.Zichichi,[9,18,19] F.Ziegler,[49]

1 I. Physikalisches Institut, RWTH, D-52056 Aachen, FRG[§]
   III. Physikalisches Institut, RWTH, D-52056 Aachen, FRG[§]
2 National Institute for High Energy Physics, NIKHEF, and University of Amsterdam, NL-1009 DB Amsterdam, The Netherlands
3 University of Michigan, Ann Arbor, MI 48109, USA
4 Laboratoire d'Annecy-le-Vieux de Physique des Particules, LAPP,IN2P3-CNRS, BP 110, F-74941 Annecy-le-Vieux CEDEX, France
5 Johns Hopkins University, Baltimore, MD 21218, USA
6 Institute of Physics, University of Basel, CH-4056 Basel, Switzerland
7 Institute of High Energy Physics, IHEP, 100039 Beijing, China[△]
8 Humboldt University, D-10099 Berlin, FRG[§]
9 University of Bologna and INFN-Sezione di Bologna, I-40126 Bologna, Italy
10 Tata Institute of Fundamental Research, Bombay 400 005, India
11 Boston University, Boston, MA 02215, USA
12 Northeastern University, Boston, MA 02115, USA
13 Institute of Atomic Physics and University of Bucharest, R-76900 Bucharest, Romania
14 Central Research Institute for Physics of the Hungarian Academy of Sciences, H-1525 Budapest 114, Hungary[‡]
15 Harvard University, Cambridge, MA 02139, USA
16 Massachusetts Institute of Technology, Cambridge, MA 02139, USA
17 INFN Sezione di Firenze and University of Florence, I-50125 Florence, Italy
18 European Laboratory for Particle Physics, CERN, CH-1211 Geneva 23, Switzerland
19 World Laboratory, FBLJA Project, CH-1211 Geneva 23, Switzerland
20 University of Geneva, CH-1211 Geneva 4, Switzerland
21 Chinese University of Science and Technology, USTC, Hefei, Anhui 230 029, China[△]
22 SEFT, Research Institute for High Energy Physics, P.O. Box 9, SF-00014 Helsinki, Finland
23 University of Lausanne, CH-1015 Lausanne, Switzerland
24 INFN-Sezione di Lecce and Universitá Degli Studi di Lecce, I-73100 Lecce, Italy
25 Los Alamos National Laboratory, Los Alamos, NM 87544, USA
26 Institut de Physique Nucléaire de Lyon, IN2P3-CNRS,Université Claude Bernard, F-69622 Villeurbanne, France
27 Centro de Investigaciones Energeticas, Medioambientales y Tecnologicas, CIEMAT, E-28040 Madrid, Spain[♭]
28 INFN-Sezione di Milano, I-20133 Milan, Italy
29 Institute of Theoretical and Experimental Physics, ITEP, Moscow, Russia
30 INFN-Sezione di Napoli and University of Naples, I-80125 Naples, Italy
31 Department of Natural Sciences, University of Cyprus, Nicosia, Cyprus
32 University of Nijmegen and NIKHEF, NL-6525 ED Nijmegen, The Netherlands
33 Oak Ridge National Laboratory, Oak Ridge, TN 37831, USA
34 California Institute of Technology, Pasadena, CA 91125, USA
35 INFN-Sezione di Perugia and Universitá Degli Studi di Perugia, I-06100 Perugia, Italy
36 Carnegie Mellon University, Pittsburgh, PA 15213, USA
37 Princeton University, Princeton, NJ 08544, USA
38 INFN-Sezione di Roma and University of Rome, "La Sapienza", I-00185 Rome, Italy
39 Nuclear Physics Institute, St. Petersburg, Russia
40 University and INFN, Salerno, I-84100 Salerno, Italy
41 University of California, San Diego, CA 92093, USA
42 Dept. de Fisica de Particulas Elementales, Univ. de Santiago, E-15706 Santiago de Compostela, Spain
43 Bulgarian Academy of Sciences, Central Lab. of Mechatronics and Instrumentation, BU-1113 Sofia, Bulgaria
44 Center for High Energy Physics, Korea Adv. Inst. of Sciences and Technology, 305-701 Taejon, Republic of Korea
45 University of Alabama, Tuscaloosa, AL 35486, USA
46 Utrecht University and NIKHEF, NL-3584 CB Utrecht, The Netherlands
47 Purdue University, West Lafayette, IN 47907, USA
48 Paul Scherrer Institut, PSI, CH-5232 Villigen, Switzerland
49 DESY-Institut für Hochenergiephysik, D-15738 Zeuthen, FRG
50 Eidgenössische Technische Hochschule, ETH Zürich, CH-8093 Zürich, Switzerland
51 University of Hamburg, D-22761 Hamburg, FRG
52 High Energy Physics Group, Taiwan, China
§ Supported by the German Bundesministerium für Bildung, Wissenschaft, Forschung und Technologie
‡ Supported by the Hungarian OTKA fund under contract numbers T14459 and T24011.
♭ Supported also by the Comisión Interministerial de Ciencia y Technología
♯ Also supported by CONICET and Universidad Nacional de La Plata, CC 67, 1900 La Plata, Argentina
◇ Also supported by Panjab University, Chandigarh-160014, India
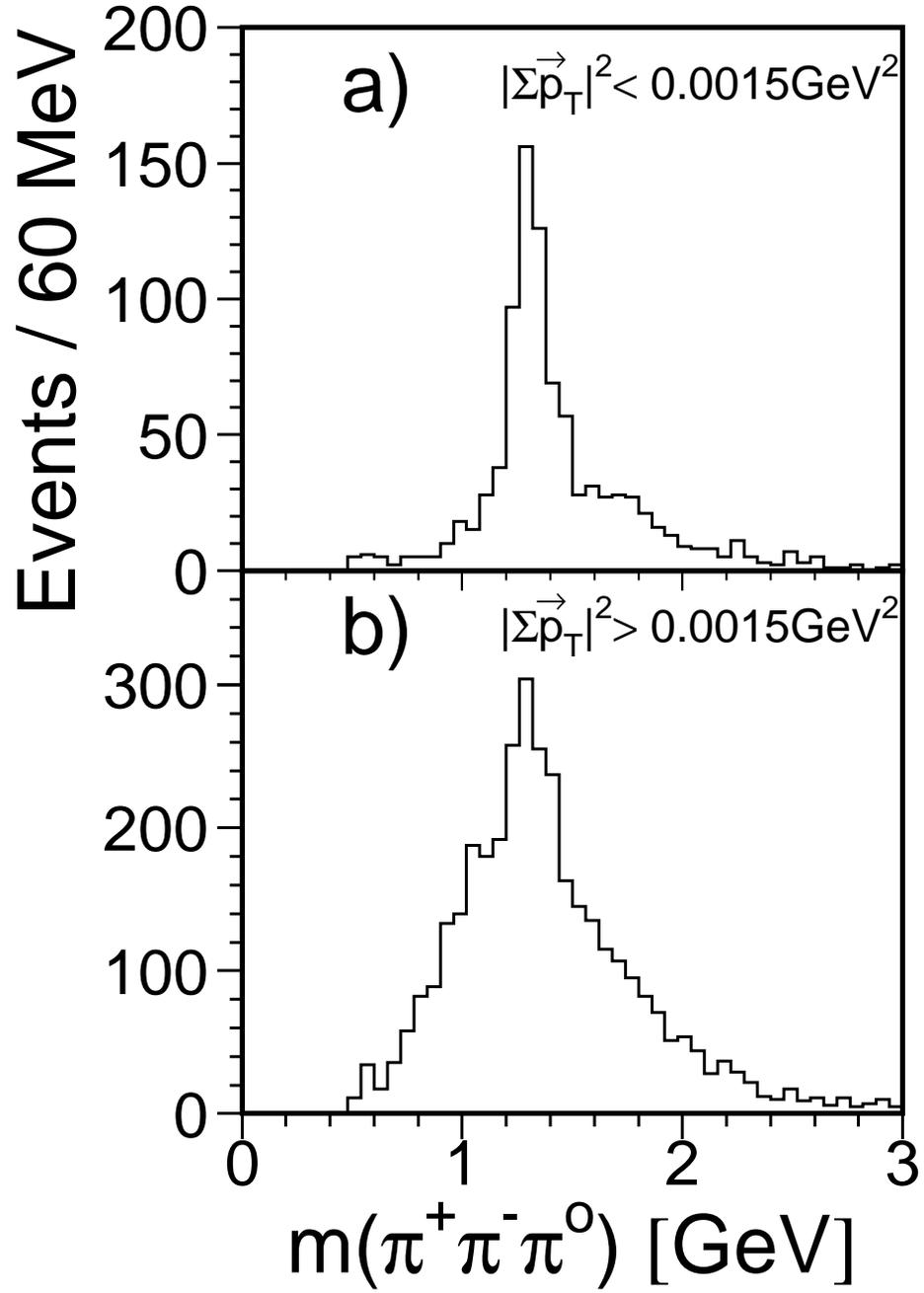△ Supported by the National Natural Science Foundation of China.

Figure 1: The $\pi^+\pi^-\pi^0$ invariant mass spectra for $|\sum \vec{p}_T|^2$ below (a) and above (b) 0.0015 GeV^2.
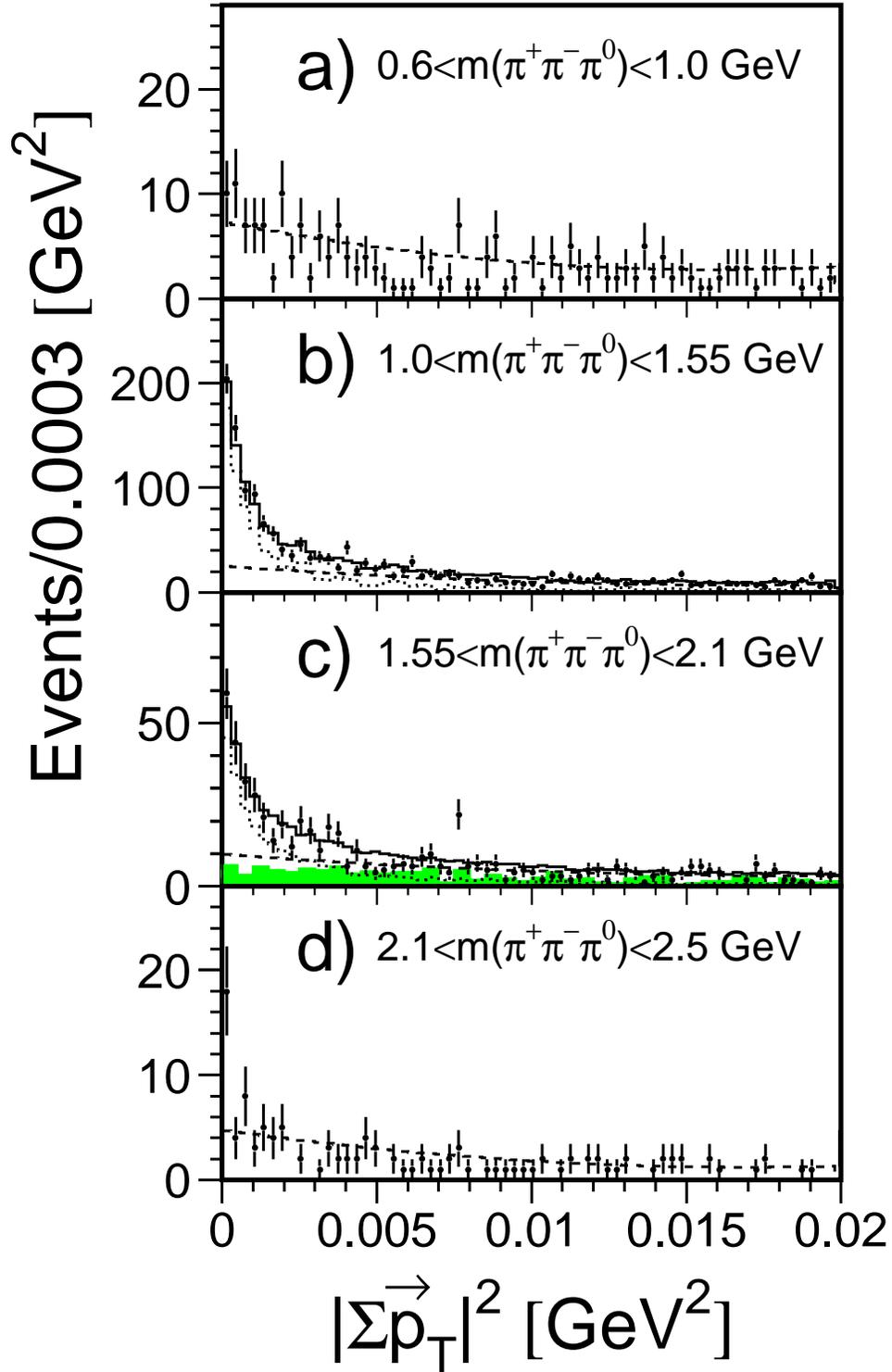
Figure 2: The $|\sum \vec{p}_T|^2$ distributions for $\pi^+\pi^-\pi^0$ events (points with statistical error) in different intervals of invariant mass. The $|\sum \vec{p}_T|^2$ distributions are fitted to background of second order polynomial (dashed line) and Monte Carlo predictions (dotted line) in b) and c) for exclusive resonance formation. The shaded histogram in c) is the distribution for a $\pi^+\pi^-\pi^0(\pi^0)$ phase space Monte Carlo sample normalized to the polynomial background estimate.
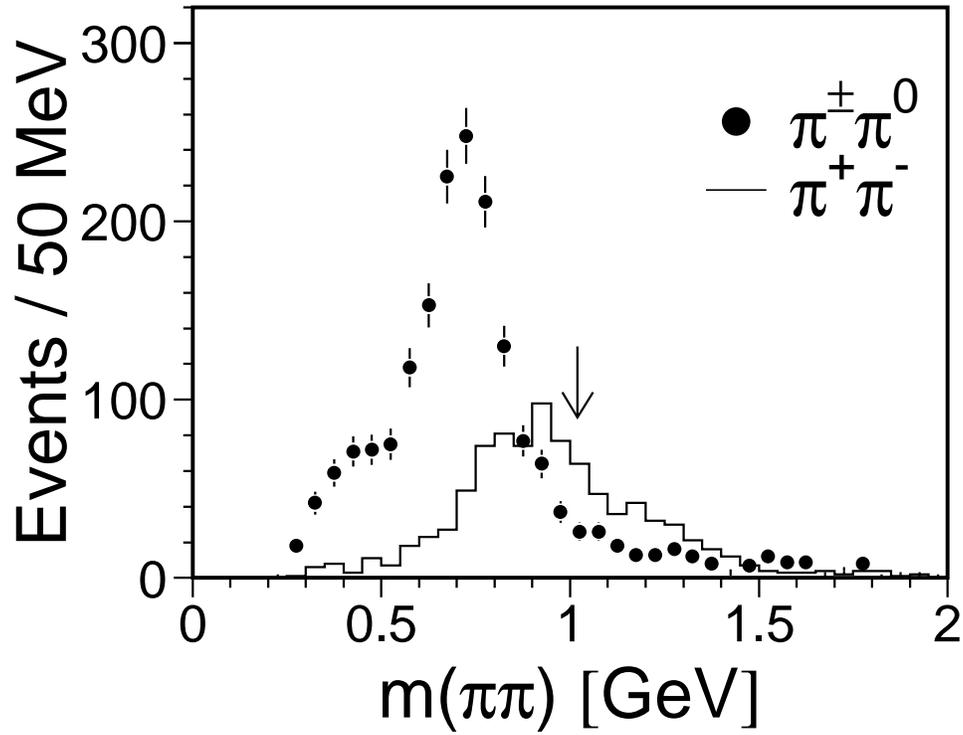
Figure 3: $\pi^{\pm}\pi^0$ (two entries per event) and $\pi^+\pi^-$ mass distributions for selected $\pi^+\pi^-\pi^0$ events. The arrow indicates the cut applied to $\pi^{\pm}\pi^0$ to define the *low-mass* sample.
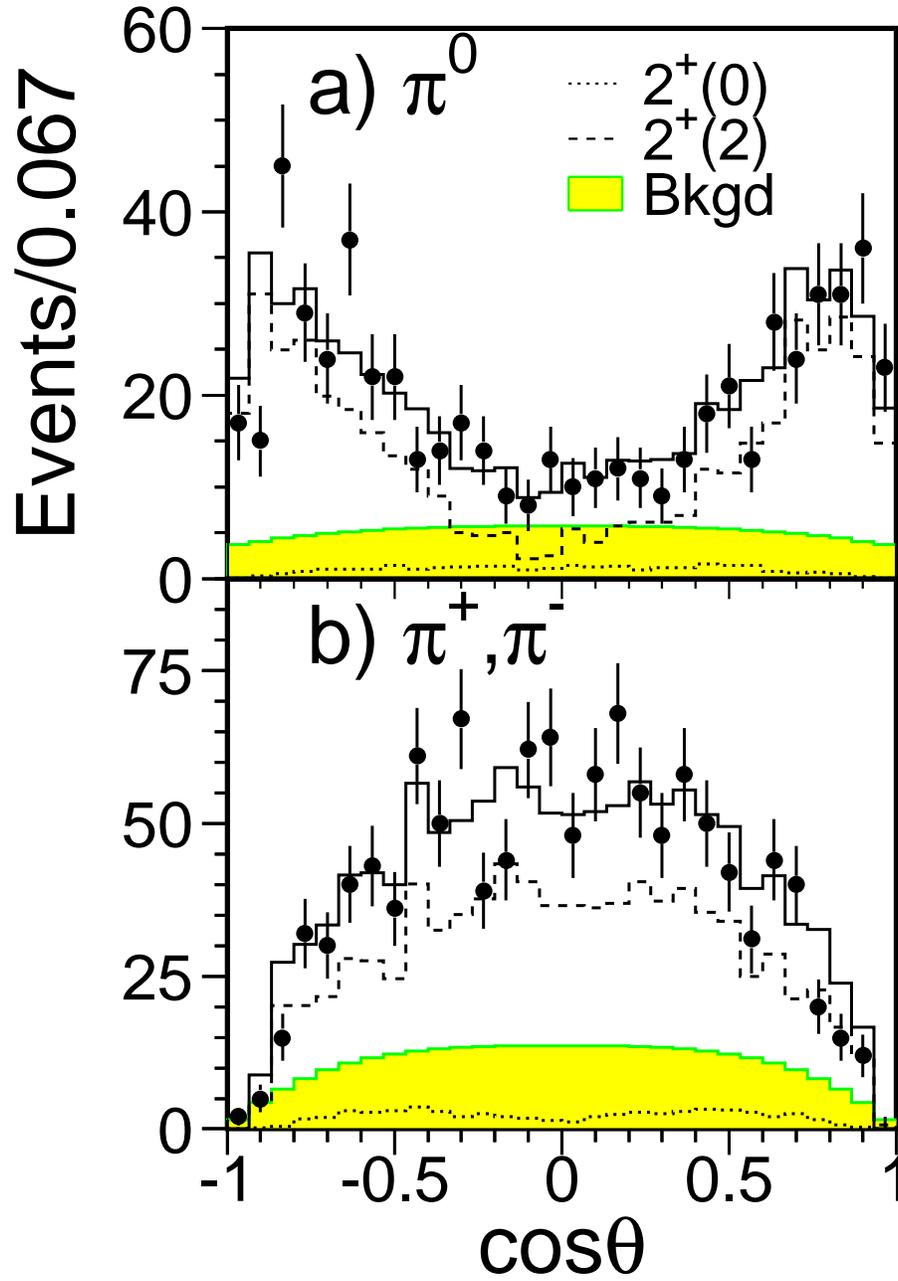
Figure 4: $\cos\theta$ distributions of a) π^0 and b) $\pi^{\pm}$ (two entries per event) for a_2 (points with statistical error) which are compared to the results of the fit (solid line). The dotted and dashed lines indicate the contributions for the two helicity states and the shaded area represents the background.
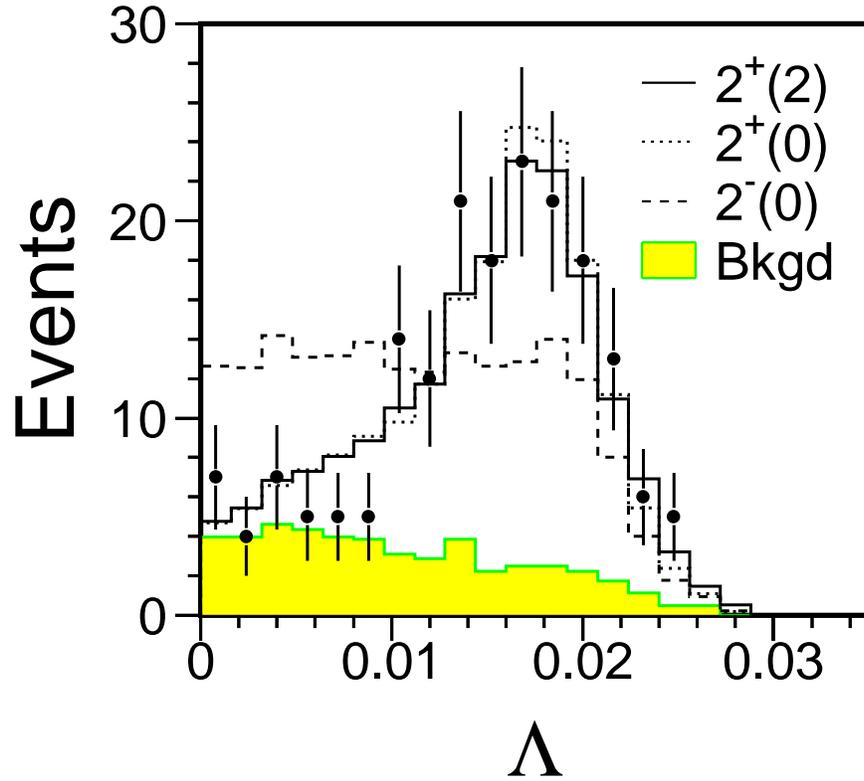
Figure 5: Λ distribution of data (points with statistical error) and Monte Carlo of $J^P(\lambda) = 2^+(0)$ (dotted), $2^+(2)$ (solid), and $2^-(0)$ (dashed), respectively. A 25% inclusive background (shaded) is included using a phase space $\pi^+\pi^-\pi^0(\pi^0)$ distribution.
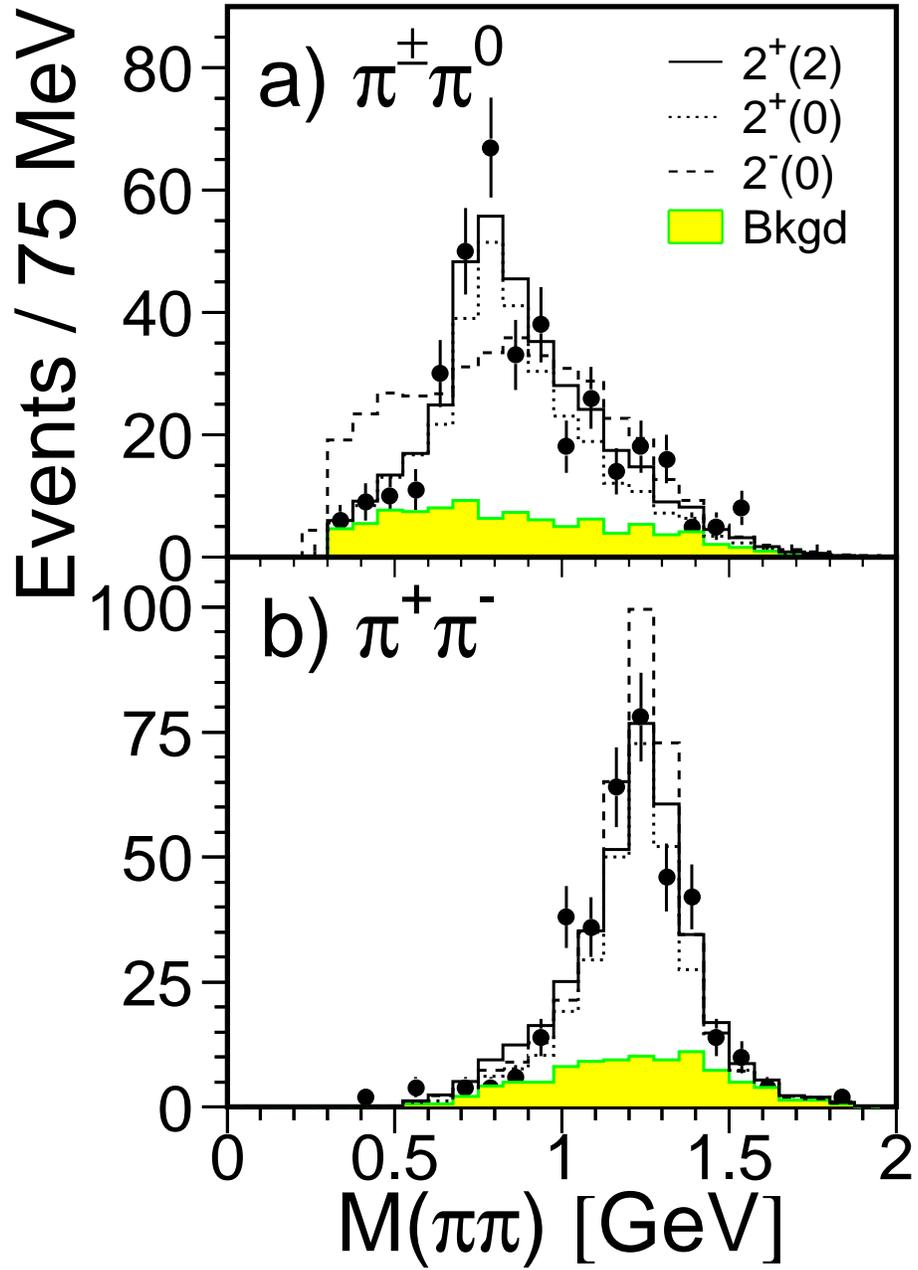
Figure 6: a) $\pi^{\pm}\pi^0$ (two entries per event) and b) $\pi^+\pi^-$ mass spectra in comparison with Monte Carlo predictions that contain 25% inclusive $\pi^+\pi^-\pi^0(\pi^0)$ background events (dashed line).
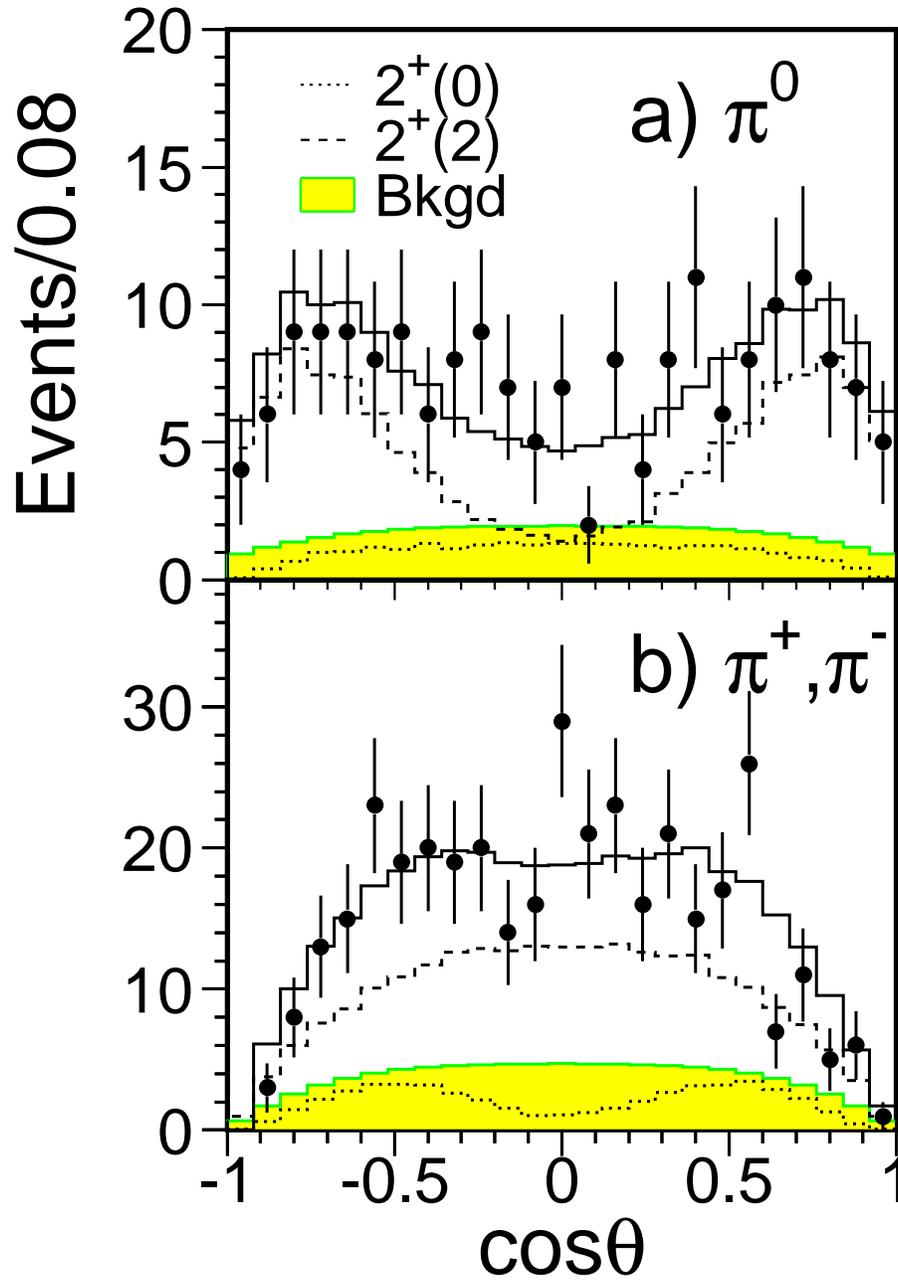
Figure 7: $\cos\theta$ distributions of a) π^0 and b) $\pi^\pm$ (two entries per event) for the *high-mass* selection (points with statistical error) which are compared to the results of the fit (solid line, column II of Table 4).
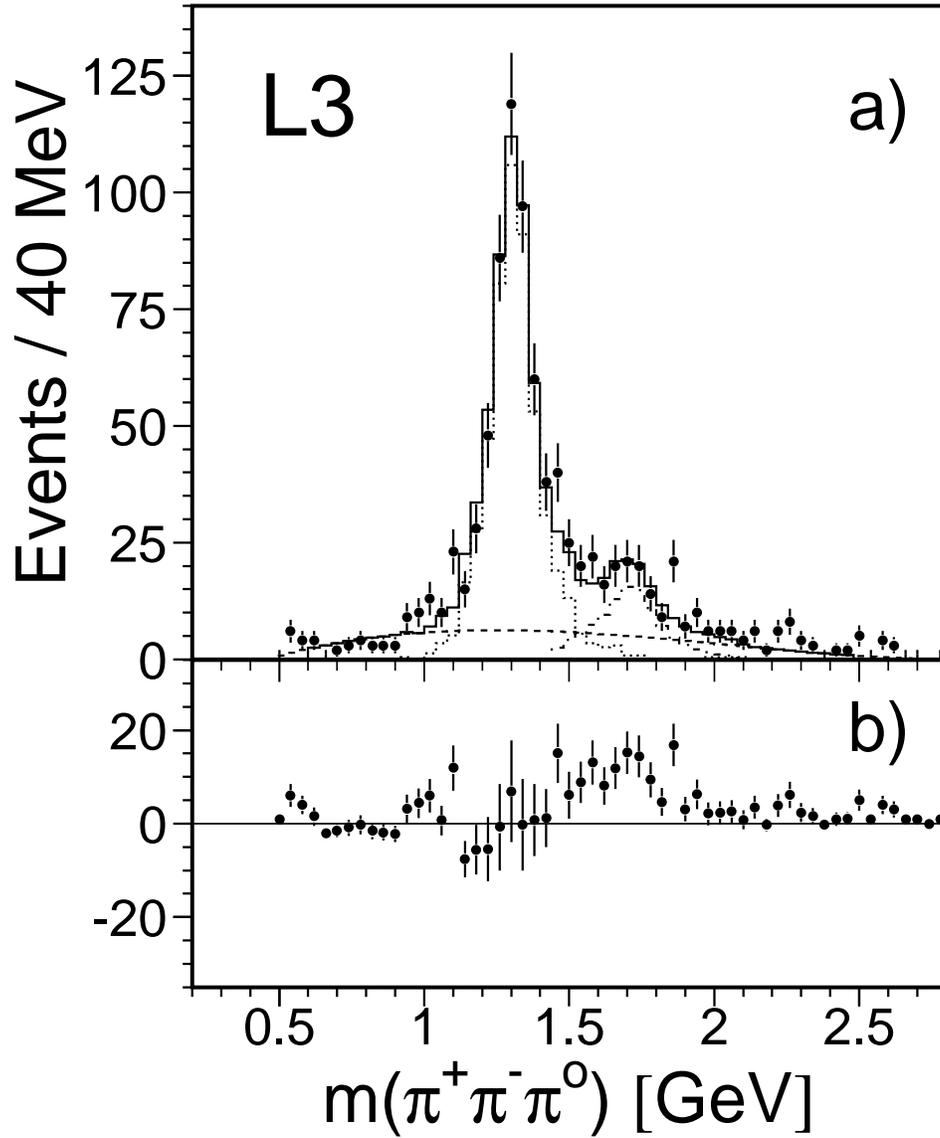
Figure 8: a) $\pi^+\pi^-\pi^0$ invariant mass spectrum; the solid line is the fit to the Monte Carlo sample for the a_2 (dotted line), a Breit-Wigner distribution in the high-mass region (dotted-dashed line) and a background parameterized by a third order polynomial (dashed line). b) the distribution with a_2 and background subtracted.